First-principles study on transport properties of zigzag graphene nanoribbon with different spin-configurations*

An Liping(安丽萍)[1,2] and Liu Nianhua(刘念华)[1,†]

[1]Institute for Advanced Study, Nanchang University, Nanchang 330031, China
[2]Department of Physics, Yanshan University, Qinhuangdao 066004, China

Abstract: The current–voltage (I–V) characteristics and the transmission spectra of zigzag graphene nanoribbon with different spin-configurations are investigated by using first-principles calculations. It is shown that the I–V curves and transmission spectra strongly depend on the spin-configurations of the two sides of the ribbon. For the spin-parallel configuration structure, the curve is linear under lower bias voltage; for the spin-antiparallel configuration structure, there is a strong spin-polarization-dependent transmission which implies that the ribbon can be used as a spin filter; while for other spin-configuration structures, the curve has the characteristics of a semiconductor. It is found that there is a large magneto-resistance (MR) when the bias voltage is small. The impurity in the central scattering region significantly influences the spin-dependent current and the spin filter efficiency, which may lead the large MR to disappear.

Key words: graphene nanoribbon; electronic transport; first-principles
DOI: 10.1088/1674-4926/32/5/052001 **PACC:** 7115M; 7225

1. Introduction

Graphene, a two-dimensional (2D) monolayer honeycomb structure of carbon, has attracted a great deal of interest since its successful preparation in 2004[1]. Due to its unique mechanical, structural, and electronic properties, graphene has potential in the applications of nanoelectronics. The charge carriers in the graphene behave like massless Dirac fermions[2]. A number of interesting phenomena, for example, Klein tunneling[3,4], ballistic transport at room temperature[5,6], and anomalous quantum Hall effects[7], are investigated. Some graphene-based devices, for example, field-effect transistors[8,9] and micromechanical resonators[10], have been proposed. These devices are directly related to the transport properties of electrons in graphene.

Graphene nanoribbons (GNRs) are quasi 1D structures cut from graphene sheet in particular orientations. They are categorized by the alignment of the edge atoms, namely, zigzag (ZGNR) and armchair (AGNR). For the ZGNR, scanning tunneling microscopy (STM) images revealed a high density of edge states near the Fermi level along its edges[11], which is important for spintronics applications. In addition, the properties of ZGNR can be changed by introducing defects[13,14], by application of gate voltage[15,16], by adsorption[17], by doping[18–23], by chemical functionalization[24,25], and by various shaped molecular junctions based on GNRs[26–32]. Since the electronic devices always work under a finite bias voltage in practice, it is necessary to study the transport properties of ZGNRs under finite bias voltage.

Based on first-principles quantum transport calculations, we investigate in this paper the current–voltage (I–V) characteristics and the transmission spectra of zigzag graphene nanoribbon with different spin-configurations. It is shown that the I–V curves and transmission spectra strongly depend on the spin-configurations of the two sides of the ribbon. For the spin-parallel configuration structure, the curve is linear under lower bias voltage; for the spin-antiparallel configuration structure, there is a strong spin-polarization-dependent transmission that implies that the ribbon can be used as a spin filter; while for other spin-configuration structures, the curve has the characteristics of a semiconductor. It is found that there is a large magneto-resistance (MR) when the bias voltage is small. The impurity in the central scattering region significantly influences the spin-dependent current and the spin filter efficiency, which may lead the large MR to disappear.

2. Model and computational method

Our modeling setups are graphene-based nanoribbon, as shown in Fig. 1. Both sides of the central scattering region are connected to two infinite electrodes (leads). The scattering region has the same structure as the electrodes. They are 4-ZGNRs with 4 zigzag chains. The spin polarization directions (arrows) can be controlled by the magnetic field. There are four different spin-configurations, as shown in Figs. 1(a)–1(d). We refer to Fig. 1(a) as P configuration in which the spin polarization directions of the two sides of the perpendicular line are parallel, and refer to Fig. 1(c) as AP configuration in which the spin polarization directions are antiparallel.

The electronic structures and the quantum transport properties are calculated by using the density-functional theory (DFT) and the nonequilibrium Green's function (NEGF) formalism implemented in the Atomistix ToolKit (ATK) package (version 2008.02)[33,34]. In our calculations, the exchange-correlation potential is described by the Perdew–Zunger local-density approximation (LDA.PZ). The Brillouin zone is sam-

* Project supported by the National Natural Science Foundation of China (No. 10832005).
† Corresponding author. Email: nhliu@ncu.edu.cn
Received 3 October 2010

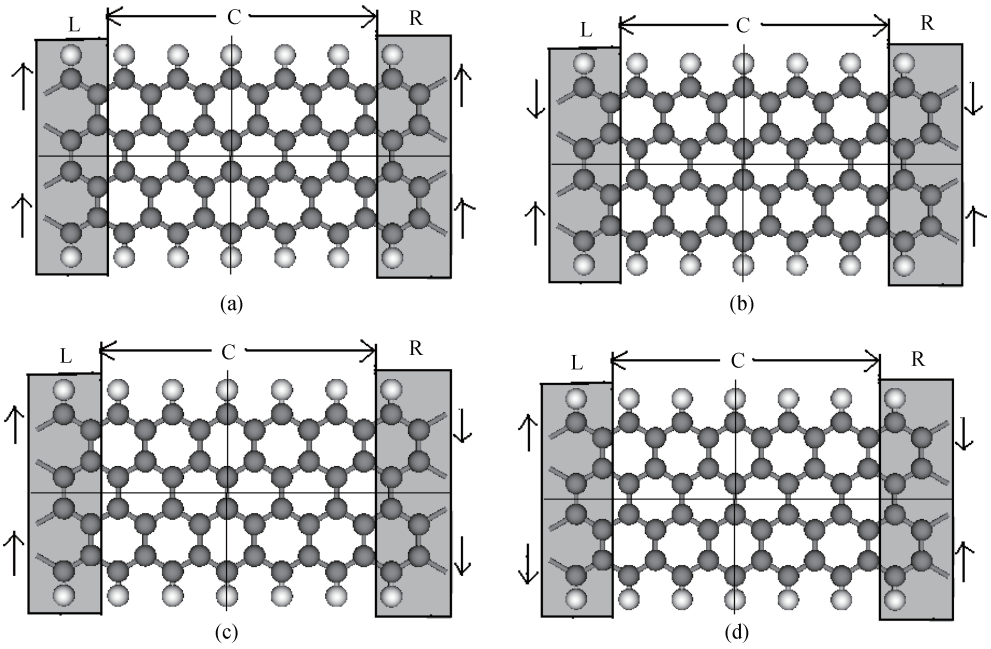

Fig. 1. 4-ZGNR, terminated by hydrogen atoms, with different spin-configurations. L, R, and C are, respectively, the left and right leads, and the central scattering region. ↑ and ↓ indicate the up-spin and down-spin. There are four different spin-configurations among four regions divided by the cross-lines. (a) P configuration. (c) AP configuration. (b), (d) Other configurations.

pled with $1 \times 1 \times 50$ k-points. A single-zeta (SZ) basis set is used and a mesh cutoff is taken to be 150 Ry to save computational time. The electron temperature is taken to be 300 K. In NEGF theory, the transmission function of the system is a sum of transmission probabilities of all channels available at energy under external bias voltage V_b[35],

$$T(E, V_b) = \mathrm{Tr}[\Gamma_L(V_b)G^R(E, V_b)\Gamma_R(V_b)G^A(E, V_b)], \quad (1)$$

where $G^{R,A}$ is the retarded and advanced Green's function. The coupling function $\Gamma_{L,R}$ is the imaginary parts of the left and right self-energies, respectively.

The I–V characteristics are obtained from the Landauer formula,

$$I(V_b) = \frac{2e}{h}\int_{-\infty}^{\infty}[f_L(E, V_b) - f_R(E, V_b)]T(E, V_b)\mathrm{d}E, \quad (2)$$

where h is Planck's constant, e is the electron charge, $f_{L/R}(E, V_b)$ is the Fermi–Dirac distribution function for the left (L)/right (R) electrode, and the difference in the electrochemical potentials is given by eV_b with the applied bias voltage V_b, i.e. $\mu_L(V_b) = \mu_L(0) - eV_b/2$ and $\mu_R(V_b) = \mu_R(0) + eV_b/2$.

3. Results and discussion

Figure 2 describes the calculated current as a function of the applied bias voltage for all four structures. The bias voltages are in the range from –1.2 to 1.2 V and in an increment step of 0.1 V. From the I–V curves, we can see that all four curves exhibit highly symmetric behavior with respect to the positive bias and negative bias due to the intrinsic symmetries of the four structures. It is interesting to note that the currents of spin-up electron and spin-down electron through the structures, as shown in Figs. 1(b) and 1(d), are degenerated completely, and the curve has the characteristics of a semiconductor. The two structures have very small currents I when $|V_b|$ is smaller than a critical bias voltage. For the P configuration shown in Fig. 1(a), the currents are degenerated partly and the curve is linear under lower bias voltage, but the currents almost saturate under larger bias voltage. However, the currents of spin-up electron and spin-down electron through the AP configuration structure shown in Fig. 1(c) are not degenerated, while they are separated completely. This structure shows half-metal behavior with spin-polarization-dependent transport properties: it behaves like a conductor to the carriers of one spin orientation, but it behaves like an insulator to those of the opposite spin orientation, as shown in Fig. 2(c). So the ribbon can be used as a spin filter. These characteristics can be understood from the following analysis of energy band gap structure.

The transmission properties are dependent on the band structure near the Fermi energy. The band structures of the electrodes or the scattering region in their primitive unit cell are shown in Fig. 3. For ZGNR, two flat bands, associated with edge states, lie at the Fermi energy if the spin is unpolarized[12]. These edge states are favor to the appearance of magnetic ordering on the edges. The spins at both edges are aligned ferromagnetically (FM) or antiferromagnetically (AF)[20]. For 4-ZGNR with AF spin configuration, a gap opens in the band structure, which means that the ZGNR becomes a semiconductor. Moreover, the spin-up band and spin-down band are degenerated. For FM spin configuration, there are two flat bands appearing at opposite sides of the Fermi energy, where the spin-up (or spin-down) flat bands are occupied (or empty) near the X point, and the energy splitting is found to be 0.455 eV at the X point. Such a band gap structure leads to metallic behavior.

The calculated zero-bias transmission spectra for four dif-

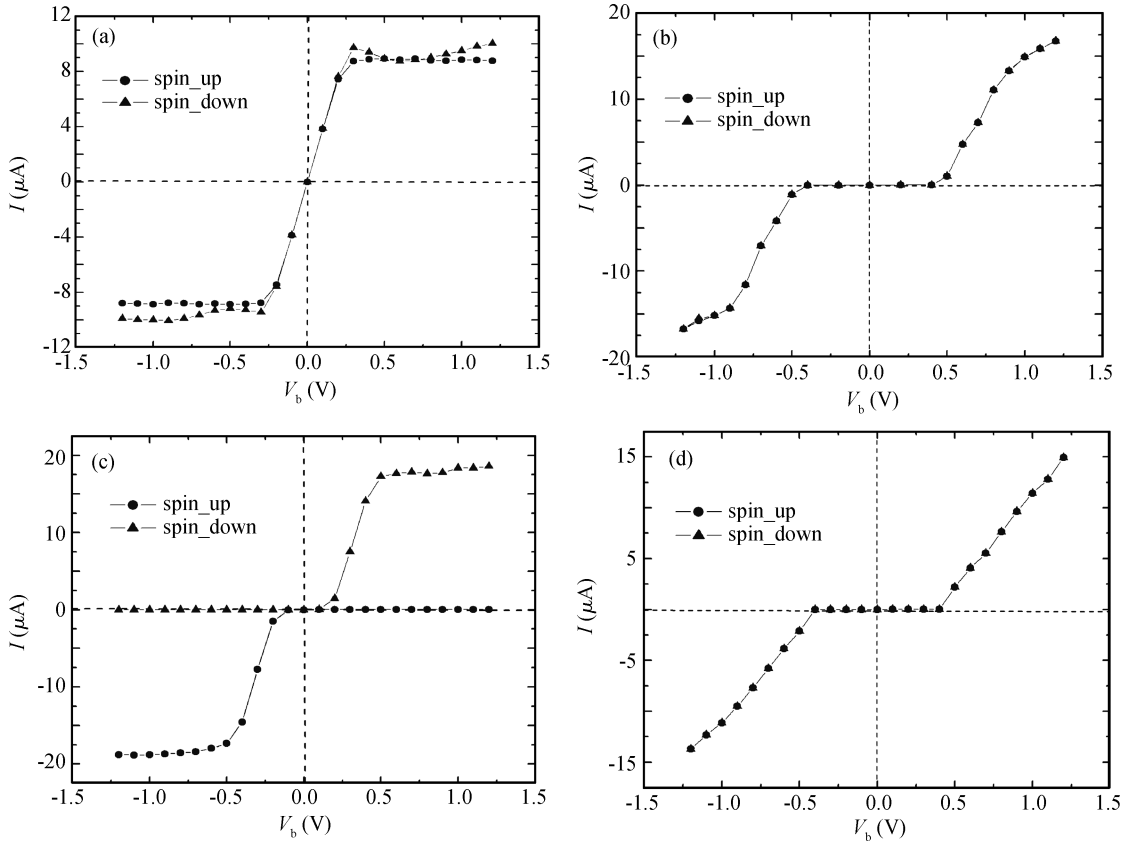

Fig. 2. I–V curves for the four structures with different spin-configurations, corresponding to the structures shown in Figs. 1(a)–1(d), respectively.

ferent structures are given in Fig. 3 (the corresponding right panels). In the P configuration shown in Fig. 1(a), the transmission spectrum shows a conventional perfect transmission. It is clear that there is no gap appearance because the band structures with the same spins are overlapped. The transmission probability remains to be one unit around the Fermi level (E_f) for both spins, as shown in Fig. 3(a). For the structures of Figs. 1(b) and 1(d), the transmission spectra of two polarizations of spins are degenerate, and a zero transmission gap appears around E_f due to the gap in the band structure, as shown in Figs. 3(b) and 3(d). Thus, a semiconducting I–V curve is formed. However, in the AP configuration shown in Fig. 1(c), the transmission spectra of two spins are also degenerate at zero bias, and a zero transmission gap appears around (E_f), which corresponds to an energy regime where the valence (conduction) state in the left panel overlaps with the conduction (valence) state for the same spin.

The spectrum of zero bias transmission is not sufficient to describe the quantum transport properties of these structures. It is necessary to consider the cases under a finite applied bias. We will pay attention to the P and AP configuration. The transmission spectra under bias voltages of 0.2, 0.4, and 0.8 V are shown in Figs. 4(a) and 4(b), respectively. As we know, the chemical potentials of the left and right leads are shifted under applied bias V_b, i.e., $\mu_L(V_b) = \mu_L(0) - eV_b/2$ and $\mu_R(V_b) = \mu_R(0) + eV_b/2$. The shaded regions in Figs. 4(a) and 4(b) correspond to the regime with different chemical potentials between the left lead and the right lead, where the electron transmission can contribute to the current flow. From Fig. 4(a), we can see that for the P configuration, as the bias increases towards the positive direction, the zero transmission gap for both spins increases monotonously. The transmission coefficient remains at one unit around the Fermi level (E_f) for both spins under lower bias, thus the I–V curve is linear. The currents almost saturate under larger bias voltage because the regime contributing to the current flow is not changed any more. For the case of AP configuration, as shown in Figs. 4(b)–4(d), when the bias increases towards the positive direction, the gap for the spin-down decreases until $V_b = 0.5$ V, where the gap is almost closed. After that, it increases. Thus, with the decrease in transmission gap, the current of spin-down increases first until $V_b = 0.5$ V, then goes to saturation since the gap opens again. However, the gap for the spin-up monotonously increases, as shown in Fig. 4(c), so that the current of spin-up is always zero. In the negative bias direction, the I–V characteristics can be explained in a similar way. Due to the nature of half-metal, it behaves like a conductor to the carriers with one spin orientation, but it behaves like an insulator to those with the opposite orientation, and the ribbon with AP configuration can be used as a spin filter.

It is found that, under low bias voltage, the current in the P configuration I_P is larger than in the AP configuration I_{AP}, as shown in Fig. 5(a). We can calculate the magnetoresistance from the I–V characteristics by using the definition in Ref. [36], MR = $(I_P - I_{AP})/I_{AP}$. The bias-voltage-dependent MR curve of 4-ZGNR at 300 K is shown in Fig. 5(b). It is found that the MR has a magnitude of 10^6% in the lower bias voltage. It increases until the bias voltage is equal approx-

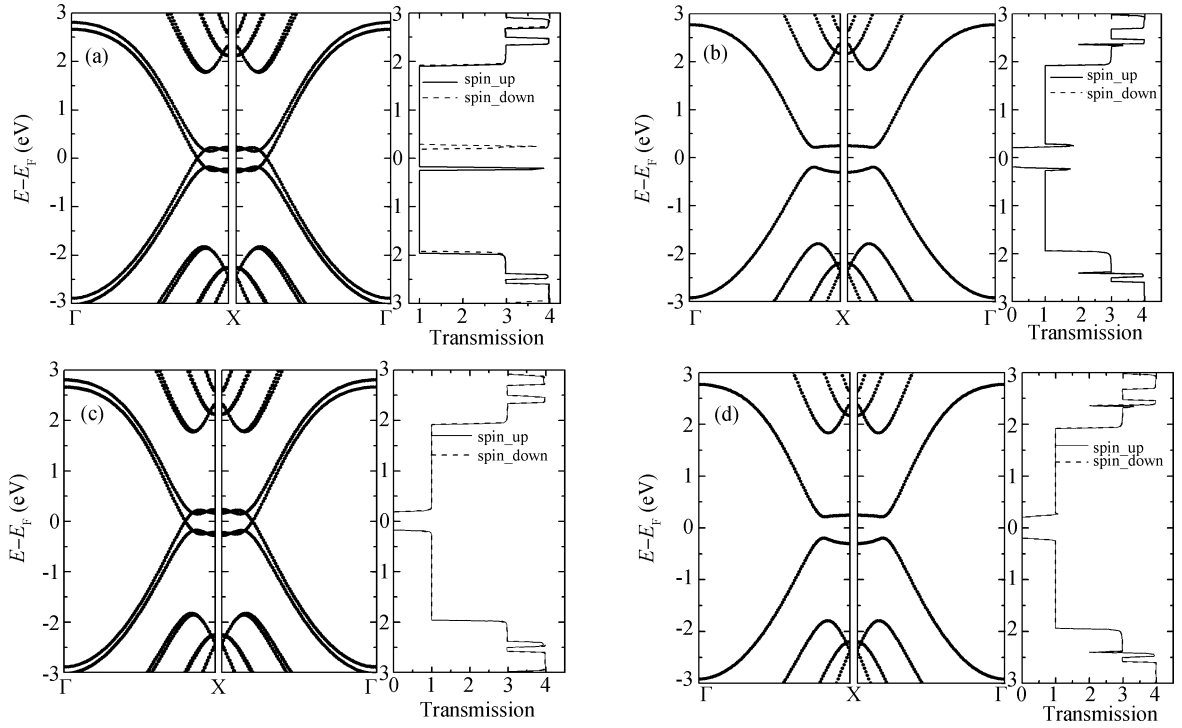

Fig. 3. Band structures of the left (L) and right (R) leads, and the corresponding spin-resolved transmission spectra (right panel) at zero bias for the four structures with different spin-configurations corresponding to Figs. 1(a)–1(d).

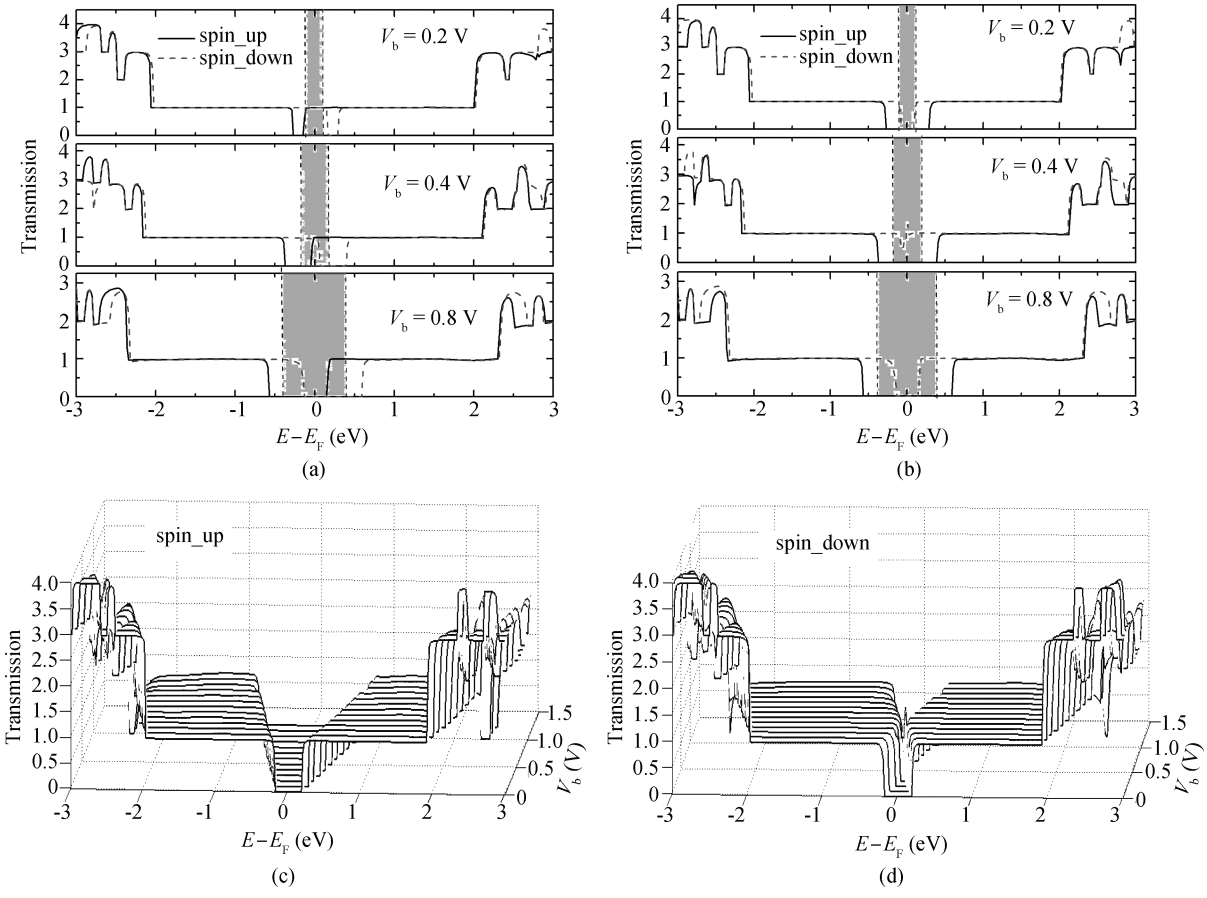

Fig. 4. Transmission spectra under different bias voltage (a) for the P configuration and (b)–(d) for the AP configuration. The shaded regions in Figs. 4(a) and 4(b) denote the area between two chemical potentials of the left and right leads.

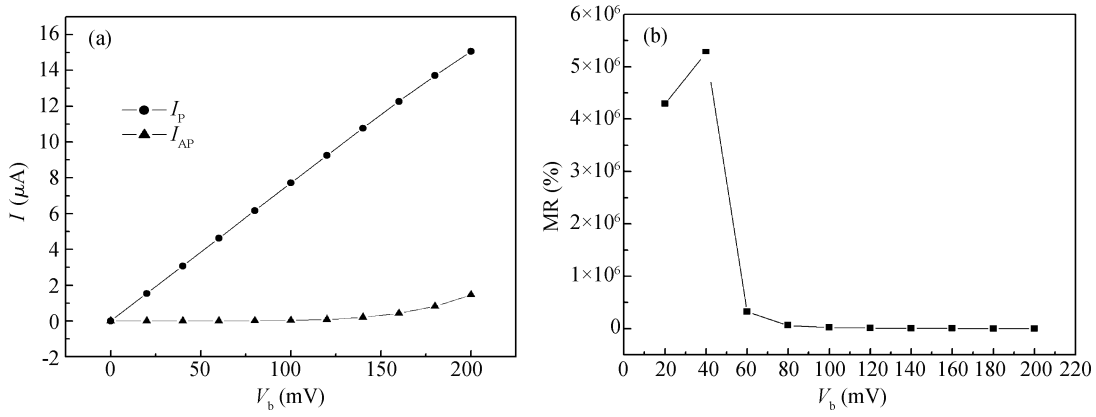

Fig. 5. I–V curves with P/AP configuration structures under small bias voltage and bias dependent magneto-resistance.

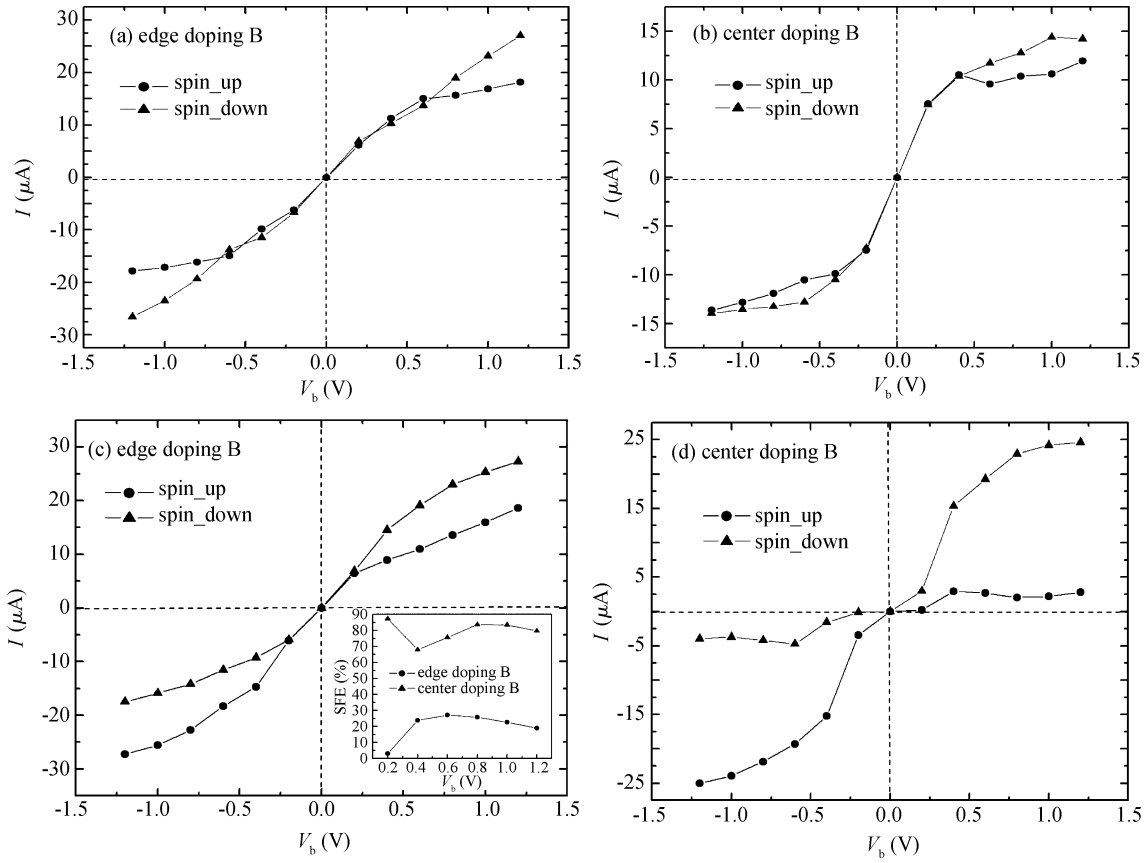

Fig. 6. I–V curves of doping B at different positions in the central region. (a), (b) For P configuration. (c), (d) For AP configuration. The inset in (c) shows the bias-voltage dependent SFE.

imately to 40 mV, then decreases.

Finally, we consider the effects of doping in the central region on the spin-polarization-dependent current and the magneto-resistance. It is found that the doping in the central region takes effects on the spin-polarization-dependent current, and thus on the spin filter efficiency, (SFE) $= \left|I_{\text{up}} - I_{\text{down}}\right| / (I_{\text{up}} + I_{\text{down}})$. For both P and AP configurations, we consider two cases of doping, edge doping and center doping. In order to save computational time, we take an increment step of 0.2 V in the bias range from –1.2 to 1.2 V. The results show that the current curve has almost not changed when one center carbon atom is substituted by a B atom, as shown in Figs. 6(b) and 6(d). When one edge carbon atom is substituted by a B atom, for the P configuration, the spin-down current curve approaches linear even under larger bias, but the current curve of spin-up is almost unchanged, as shown in Fig. 6(a). However, for the AP configuration, the current of spin-up is a finite value, as shown in Fig. 6(c), thus the spin filter efficiency is much lower, as shown in the inset of Fig. 6(c).

4. Conclusion

In summary, by using first-principles calculations, we have investigated the I–V characteristics and the transmis-

sion spectra of zigzag graphene nanoribbon with different spin-configurations. It is shown that the I–V curves and the transmission spectra strongly depend on the spin-configurations of the two sides of the ribbon. For the P configuration structure, the curve is linear under lower bias voltage. For the AP configuration structure, transport is spin-polarization-dependent, so that the ribbon can be used as a spin filter. For other spin-configurations, the curve has the characteristics of a semiconductor. Under low bias voltage, the current in the P configuration I_{P} is much larger than in the AP configuration, which results in a large magneto-resistance. We have also considered the effects of doping in the central region on the spin-polarized current and the large magneto-resistance. The results show that the impurity influences significantly the spin-polarization-dependent current and thus the spin filter efficiency, and can cause the large magneto-resistance to disappear.

Acknowledgments

We wish to thank Atomistix for the use of the trial version of Atomistix ToolKit 2.3 (ATK 2.3).

References

[1] Novoselov K S, Geim A K, Morozov S V, et al. Electric field effect in atomically thin carbon films. Science, 2004, 306: 666
[2] Novoselov K S, Geim A K, Morozov S V, et al. Two-dimensional gas of massless Dirac fermions in graphene. Nature (London), 2005, 438: 197
[3] Katsnelson M I, Novoselov K S, Geim A K. Chiral tunneling and the Klein paradox in graphene. Nat Phys, 2006, 2: 620
[4] Young A F, Kim P. Quantum interference and Klein tunneling in graphene heterojunctions. Nat Phys, 2009, 5: 222
[5] Gunlycke D, Lawler H M, White C T. Room-temperature ballistic transport in narrow graphene strips. Phys Rev B, 2007, 75: 085418
[6] Du X, Skachko I, Barker A, et al. Approaching ballistic transport in suspended graphene. Nat Nanotechnol, 2008, 3: 491
[7] Novoselov K S, Jiang Z, Zhang Y, et al. Room-temperature quantum hall effect in graphene. Science, 2007, 315: 379
[8] Wang X, Ouyang Y, Li X, et al. Room-temperature all-semiconducting sub-10-nm graphene nanoribbon field-effect transistors. Phys Rev Lett, 2008, 100: 206803
[9] Lin Y M, Dimitrakopoulos C, Jenkins K A, et al. 100-GHz transistors from wafer-scale epitaxial graphene. Science, 2010, 327: 662
[10] Bunch J S, van der Zande A M, Verbridge S S, et al. Electromechanical resonators from graphene sheets. Science, 2007, 315: 490
[11] Kobayashi Y, Fukui K I, Enoki T, et al. Edge state on hydrogen-terminated graphite edges investigated by scanning tunneling microscopy. Phys Rev B, 2006, 73: 125415
[12] Son Y W, Cohen M L, Louie S G. Energy gaps in graphene nanoribbons. Phys Rev Lett, 2006, 97: 216803
[13] Ouyang F P, Huang B, Li Z Y, et al. Chemical functionalization of graphene nanoribbons by carboxyl groups on stone-wales defects. J Phys Chem C, 2008, 112: 12003
[14] Zheng X H, Zhang G R, Zeng Z, et al. Effects of antidots on the transport properties of graphene nanoribbons. Phys Rev B, 2009, 80: 075413
[15] Fernández-Rossier J, Palacios J J, Brey L. Electronic structure of gated graphene and graphene ribbons. Phys Rev B, 2007, 75: 205441
[16] Cresti A, Grosso G, Parravicini G P. Numerical study of electronic transport in gated graphene ribbons. Phys Rev B, 2007, 76: 205433
[17] Choi S M, Jhi S H. Self-assembled metal atom chains on graphene nanoribbons. Phys Rev Lett, 2008, 101: 266105
[18] Dutta S, Pati S K. Half-metallicity in undoped and boron doped graphene nanoribbons in the presence of semilocal exchange-correlation interactions. J Phys Chem B, 2008, 112: 1333
[19] Cervantes-Sodi F, Csányi G, Piscanec S, et al. Edge-functionalized and substitutionally doped graphene nanoribbons: electronic and spin properties. Phys Rev B, 2008, 77: 165427
[20] Martins T B, Miwa R H, da Silva A J R, et al. Electronic and transport properties of boron-doped graphene nanoribbons. Phys Rev Lett, 2007, 98: 196803
[21] Biel B, Blase X, Triozon F, et al. Anomalous doping effects on charge transport in graphene nanoribbons. Phys Rev Lett, 2009, 102: 096803
[22] Zheng X H, Rungger I, Zeng Z, et al. Effects induced by single and multiple dopants on the transport properties in zigzag-edged graphene nanoribbons. Phys Rev B, 2009, 80: 235426
[23] Zheng X H, Wang R N, Song L L, et al. Impurity induced spin filtering in graphene nanoribbons. Appl Phys Lett, 2009, 95: 123109
[24] Boukhvalov D W, Katsnelson M I. Chemical functionalization of graphene with defects. Nano Lett, 2008, 8: 4373
[25] Pisani L, Chan J A, Montanari B, et al. Electronic structure and magnetic properties of graphitic ribbons Harrison. Phys Rev B, 2007, 75: 064418
[26] Cheraghchi H, Esfarjani K. Negative differential resistance in molecular junctions: application to graphene ribbon junctions. Phys Rev B, 2008, 78: 085123
[27] Andriotis A N, Richter E, Menon M. Strong dependence of transport properties of metal–semiconductor–metal graphene ribbons on their geometrical features. Appl Phys Lett, 2007, 91: 152105
[28] Hong S, Yoon Y, Guo J. Metal–semiconductor junction of graphene nanoribbons. Appl Phys Lett, 2008, 92: 083107
[29] Wang B, Wang J, Guo H. *Ab initio* calculation of transverse spin current in graphene nanostructures. Phys Rev B, 2009, 79: 165417
[30] Topsakal M, Sevinçli H, Ciraci S. Spin confinement in the superlattices of graphene ribbons. Appl Phys Lett, 2008, 92: 173118
[31] ZhangY T, Jiang H, Sun Q F, et al. Spin polarization and giant magnetoresistance effect induced by magnetization in zigzag graphene nanoribbons. Phys Rev B, 2010, 81: 165404
[32] Ozaki T, Nishio K, Weng H M, et al. Dual spin filter effect in a zigzag graphene nanoribbon. Phys Rev B, 2010, 81: 075422
[33] Brandbyge M, Mozos J L, Ordejon P, et al. Density-functional method for nonequilibrium electron transport. Phys Rev B, 2002, 65: 165401
[34] Taylor J, Guo H, Wang J. *Ab initio* modeling of quantum transport properties of molecular electronic devices. Phys Rev B, 2001, 63: 245407
[35] Datta S. Electronic transport in mesoscopic system. New York: Cambridge University Press, 1995
[36] Zeng M G, Shen L, Cai Y Q, et al. Perfect spin-filter and spin-valve in carbon atomic chains. Appl Phys Lett, 2010, 96: 042104